

WIND EFFECTS ON WAVE OVERTOPPING AT THE VERTICAL SEA DEFENCE

S De Chowdhury¹, J. G. Zhou, L. Qian, D. Causon, C. Mingham², T. Pullen³, K Hu⁴, M Russell, S Manson⁵, D Stewart, M Wood⁶, H Winter, A. Joly⁷

Wind effects on wave overtopping over fully impermeable vertical sea defence is studied in a shallow water flume based on a physical model for the Livermeade defence system. The investigation is mainly focused on impulse type wave interaction with the sea defence, when the overshooting jet is high during overtopping. We are able to identify distinct types of overtopping flows where moderate wind speed is not found to be affecting uniformly in all cases. We try to find explanation of this behaviours by studying the standing waves at the defence and complementary CFD simulations.

Keywords: wave overtopping; wind effects; wave structure interactions; wave impacts; OpenFOAM

INTRODUCTION

Many coasts are vulnerable to wind effects at moderate to high wind speeds during normal weather as well as a storm surge. Coastal defences are standard choices to protect the coasts against flooding from wave overtopping and yet still it is not usual to design them based on studies specifically focused on an understanding of wind effects. The primary reason is that the incorporation of a wind generation facility into an existing physical flume is not straightforward.

There are studies to account for wind effects on overtopping in physical model tests. For example, De Waal et al. (1996) and Wolters and van Gent (2007) used paddle wheels rotated at a given speed to transport water spray generated due to the wave impact on the vertical structure. These tests suggested a high increase in overtopping rates by wind compared to no wind conditions in some specific types of wave impacts, although results could not be quantified fully due to the lack of proper scaling laws. González-Escrivá et al. (2004) reproduced a real storm surge event in a laboratory and reported a significant increase in overtopping rates due to wind especially on small overtopping rates. One can predict wind effects on overtopping (De Rouck et al. (2005)) using estimates from neural network models (van Gent et al. (2007)) based on a large database created from numerous physical model tests. This can give certain factors to scale the overtopping rates without wind to account for wind effects. However, sometimes it is hard to find a physical explanation behind this scaling. As there is no reliable empirical relations for accessing wind effects on wave overtopping, coastal engineers are left with prescribing a wide margin in the design of a coastal defence-height. This appears to be a normal choice for places with high onshore wind speeds in particular, but clearly less economical in practice. Thus although much effort have been spent on understanding the wave structure interactions in overtopping under typical ambient condition with negligible or no wind speed, clearly our knowledge about wind effects on overtopping is far from being fully developed.

In this paper, we try to improve our current understanding on this topic by conducting new physical model tests and developing new CFD tools to provide conclusive support for the data from the tests. The tests are performed at the Froude Hydrodynamics Laboratory at the HR Wallingford for their branch in Oxfordshire which has state of the art facilities for conducting experiments in Coastal Engineering. In this paper, firstly we describe the set up and the incident wave conditions for the physical model tests. We then discuss sample data from some of these tests and show the variation in the wind effect on wave overtopping subjected to change in the incident wave condition (namely the wave steepness and the impulse parameter. We make hypothesis to explain our findings from the physical tests wherever possible and we are able to support that with results from our multiphase CFD simulations.

EXPERIMENTS AT HR WALLINGFORD

The experiments are conducted in a shallow water flume at the Froude hydrodynamics laboratory at HR Wallingford. Details of the bathymetry of this flume is shown in Figure 1 in model scale. We fabricated a sea

¹Risk Management Solutions, London, UK

²Centre for Mathematical Modelling and Flow Analysis, Department of Computing and Mathematics, Manchester Metropolitan University, Manchester, UK

³HR Wallingford, Oxfordshire, UK

⁴Royal HaskoningDHV, UK

⁵Environment Agency, UK

⁶Torbay Council, UK

⁷EDF Energy RD UK Centre, UK

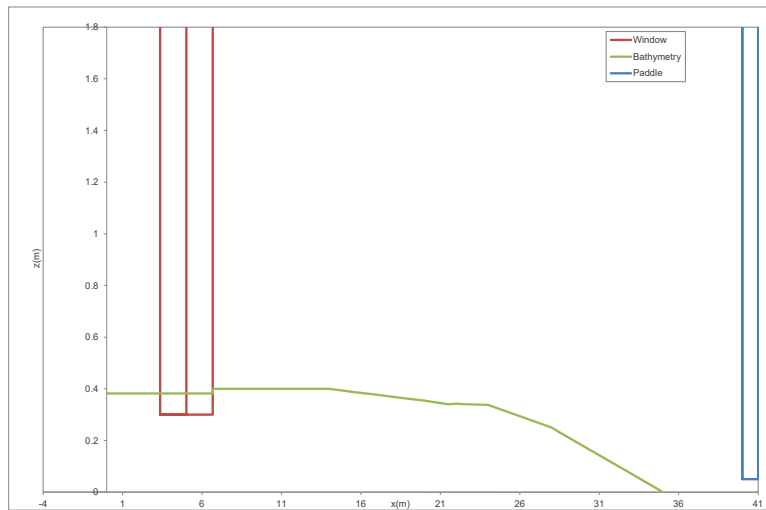


Figure 1: Bathymetry of the shallow water flume.

defence model replicating the Livermeade profile at 1 : 17 model to prototype scale. The placement of the sea defence model in the flume is shown in Figure 2(a). We place two rows of fans in front of the sea defence model. The power input to these fans are controlled using wind dial gauges and so different readings of these dials refer to different input wind speeds we wish to achieve near the sea defence. The overtopping water is collected inside a tank placed just after the defence model. The tank has many separate compartments and the water level rise in each of these during overtopping events is measured using the dip sticks as shown in Figure 2(b). We carefully extract the overtopping water by pumps when the compartments get filled and the extracted water volume is duly accounted for while calculating the overtopping discharges per unit crest widths based on the data measured by the dip sticks. We cover a range of wave conditions, with an sample as shown in Table 1 to be as close as a real sea state and achieve statistically significant results for the overtopping rates.

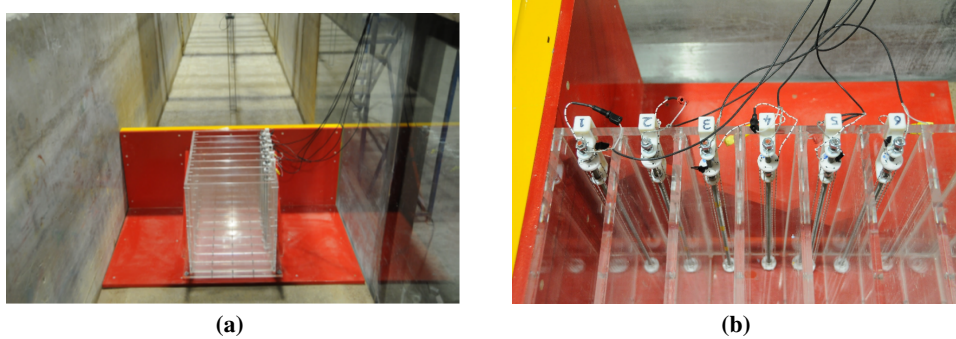


Figure 2: (a) Tank after the defence model to collect overtopping water and (b) the dip sticks inside the tank compartments.

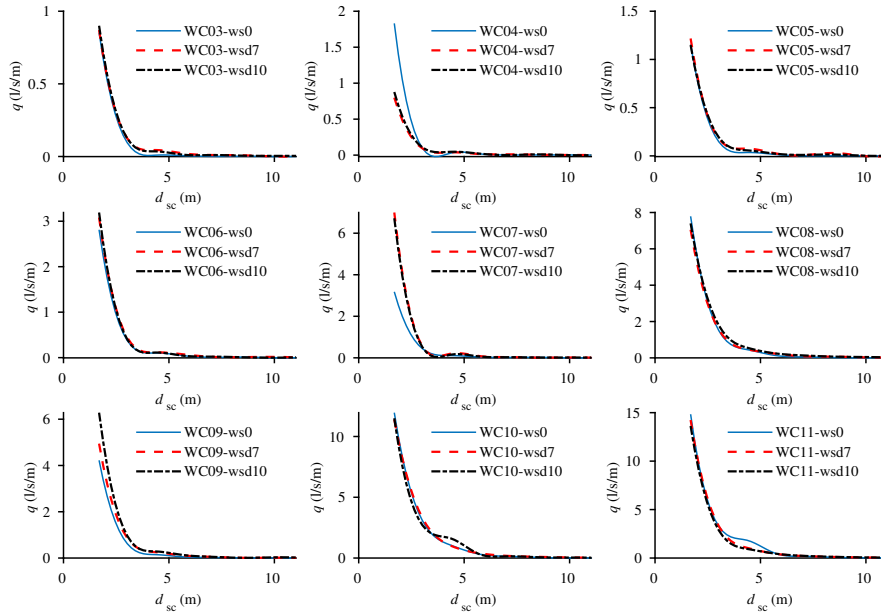


Figure 3: Overtopping rates measured across distance from the sea defence crest.

Table 1: Sample incident wave conditions used in the physical model tests, where H_{m0} and T_p are the spectral wave height and peak wave periods respectively for combination of Still Water Levels (SWL) leading to various impulse parameters \mathcal{I} .

| Incident wave condition | SWL(m) | H_{m0} (m) | T_p (s) | \mathcal{I} |
|-------------------------|--------|--------------|-----------|---------------|
| WC03 | 2.31 | 2.44 | 11.0 | 0.021 |
| WC04 | 2.31 | 2.41 | 10.5 | 0.022 |
| WC05 | 2.31 | 2.46 | 12.0 | 0.017 |
| WC06 | 3.0 | 2.55 | 9.72 | 0.04 |
| WC07 | 3.0 | 2.66 | 10.0 | 0.038 |
| WC08 | 3.3 | 2.85 | 10.22 | 0.041 |
| WC09 | 3.3 | 2.66 | 9.57 | 0.046 |
| WC10 | 3.5 | 2.80 | 9.92 | 0.045 |
| WC11 | 3.5 | 2.89 | 10.07 | 0.043 |

Our choice for the various wave conditions is primarily based on the impulse parameter \mathcal{I} which is given as Van der Meer et al. (2018)

$$\mathcal{I} = \frac{h^2}{H_{m0}\lambda_{m-1,0}}, \quad (1)$$

where h is the initial water depth at the toe of the sea defence and $\lambda_{m-1,0}$ is the deep water wave length. When $\mathcal{I} \leq 0.23$, the wave interaction with the sea defence leads to a high overshoot and the probability of significant wind effect on overtopping increases. Thus the impulse parameter helps us to choose the right incident wave conditions for our test cases.

Variation in the overtopping rates over distance from the sea defence

One of the direct actions of wind on overtopping is that the overtopping water is dragged much inland due to wind speed. The arrangement of the dip sticks in the overtopping tank (as shown in Figure 2(b)) allows us to investigate that process. The variation in the overtopping rates over the distance d_{sc} from the sea defence crest under various wave conditions (as provided in Table 1) is shown in Figure 3 in prototype scale. Here wsd7 and wsd10 refer to two different wind dial readings, i.e., wind speeds of 1.4m/s and 1.7m/s. Whereas, ws0 refers to cases when the imposed wind speed is zero. From Figure 3, we can clearly distinguish three different types overtopping that is taking place. Overtopping of Type A (e.g., WC03,

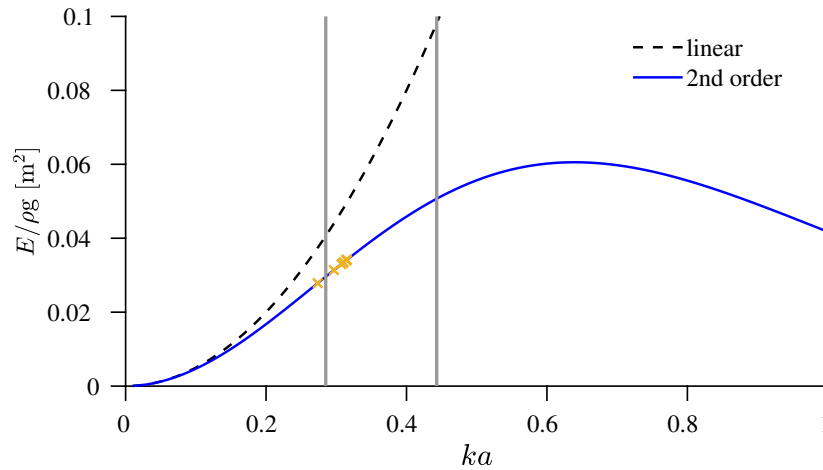


Figure 4: Linear and second order standing wave energy (E , non dimensionalized by water density ρ and acceleration due to gravity g) over the wave steepness. The two vertical lines denote the region of the critical wave steepness, i.e., (0.285, 0.443). Individual cases from the physical model tests are marked with \times where the leftmost point refers to WC03 and rightmost point refers to WC11.

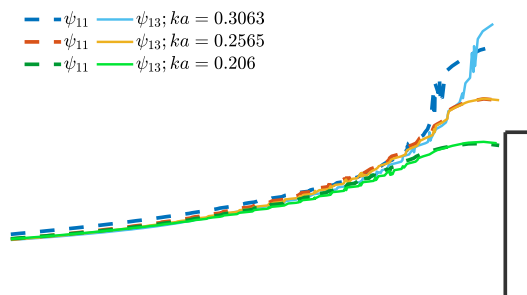


Figure 5: Form of the overshooting jets under different wave steepness but same impulse parameter at the vertical sea defence. ψ_{11} and ψ_{13} refers to the first and the third of the three consecutive wave cycles.

WC05 and WC10), where the wind effects on wave overtopping is marginal; overtopping of Type B (e.g., WC04, WC08 and WC11), where apparently there is a reduction in overtopping discharges adjacent to the sea defence under the action of wind speeds and overtopping of Type C (e.g., WC06, WC07 and WC09) where there are clear evidence of higher overtopping discharges in the presence of wind speeds. The wave interactions in each of these categories has some distinct features which is of some interest to investigate.

Shape of the overshooting jet due to standing wave instability

The overshooting jet due to a impulse type wave interaction depends greatly on the stability of the standing wave field at the vertical sea defence. This is firstly noticed experimentally by Longuet-Higgins and Drazen (2002) who find that when the steepness ka (where k and a are the wave number and wave amplitude at the vertical sea defence) of the incident wave is in the range (0.285, 0.443), the resulting standing wave at a fully impermeable vertical structure is unstable, often leading to triplets where each of the third wave is the highest among three consecutive wave cycles impinging on the structure. The various wave steepness deduced from the physical model tests is depicted in Figure 4.

We can verify the occurrence of the standing wave instability using CFD simulations (details in Appendix) as in Figure 5, where we compare the overshooting jets under ka with one (i.e., $ka = 0.3063$) being inside the critical wave steepness and other two outside of it which are representative of case WC03. For kind of interactions of that in WC03 (i.e., overtopping type A), the overshooting jet is mild and thick and

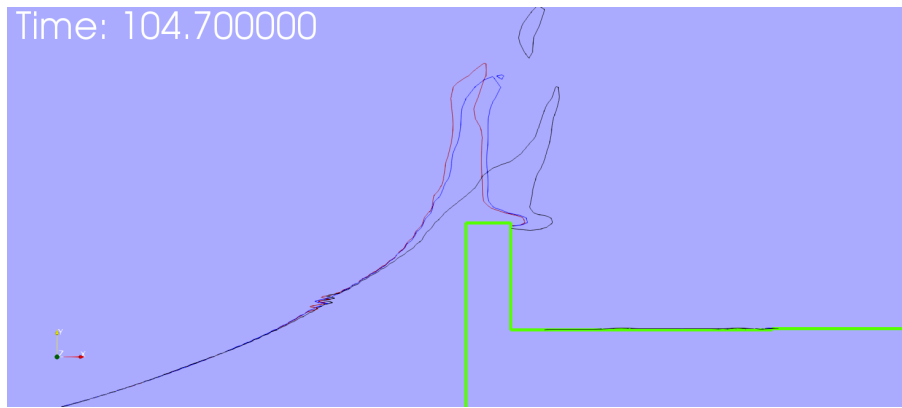


Figure 6: Overshooting jets in Type A and Type B overtopping. The case in red line shows the jet in Type A with zero wind speed, whereas, the case in blue is for Type A with low wind speed in Type A. The profile in black shows the overshooting jet under wind speed in Type B.

the low wind speed does not have sufficient kinetic energy to alter it, specifically at the crest of the sea defence. However, as the jet collapses under the action of gravity, the smaller fragments of the jet are easily dragged inland. Therefore the wind effects are more noticeable at some distance from the sea defence. This is reflected in overtopping discharges in Type A, around 5m from the sea defence. The wave steepness in cases WC05 and WC10 are inside critical wave steepness regime, but has higher impulse parameters than in case WC03. We have chances of instability in these cases, but most likely with thicker jets. Thus the overtopping of Type A is characterized by sub critical wave steepness and high impulse parameter, or thick overshooting jet.

The overtopping in Type B is rather less intuitive. All of these cases are well within critical wave steepness and therefore shows interactions of kind as we see in Figure 5 for $ka = 0.3063$. The overshooting jet is very high at each of the third wave (i.e., ψ_{13} of each cycle) and also very wide at the base due to high impulse parameter (specifically for WC08 and WC11). In the absence of wind, most portion of this jet falls on the first tank immediately after the sea defence. Whereas, in the presence of wind, the mid portion of the jet is carried bit inland and this portion of fluid eventually falls in the second, third tanks or afterwards starting from the sea defence. Thus in Type B, we have higher wind effects away from the sea defence. From engineering point of view, information about this type of overtopping may be very useful, since in practice many of the existing transport links pass by a nearby coastal defence system. Better insight of Type A and Type B overtopping can be gained from results from our CFD simulations and this is shown in Figure 6.

In overtopping of Type C, all of these cases are within critical wave steepness as well, but have uniform thinner overshooting jets at the sea defence. The wind speeds achieved in the tests are able to act on it uniformly over the entire length of the jet and causes the water level in the tanks to rise at much faster rate than in the absence of wind. This also shows that the the overtopping discharges can be as high as almost two times (i.e., case WC04) of that without wind, immediately after the sea defence.

EFFECT OF INCIDENT WAVE HEIGHT AND SEA DEFENCE CREST HEIGHT ON OVERTOPPING

The variation in the overtopping rates over the choice of crest level of the sea defence is shown in Figure 7. We can interpret this result based on the discussion on the various type of overtopping in the above section. When the incident wave height is high (small R_c/H_{m0}), the overshooting jet is thick and the wind effects are small. Whereas, at the higher end of R_c/H_{m0} , the incident wave height is smaller and there is greater mixing of air. The wind effects are higher in overtopping in these cases in particular. There is some region in between where we find significant wind effects on overtopping and we need more investigations using our CFD model on that. This is under progress and will be presented elsewhere.

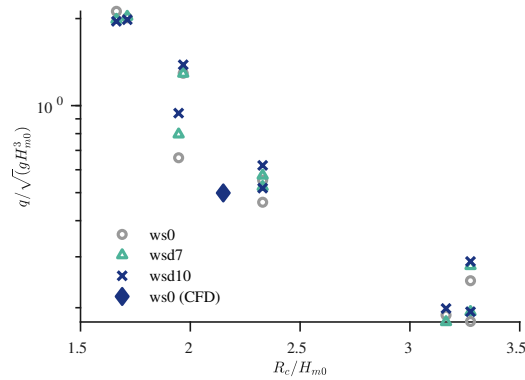


Figure 7: Variation in the overtopping rate over sea defence crest level R_c nondimensionalized by incident spectral wave height H_{m0} .

CONCLUSION

In this paper we report some preliminary results investigating wind effects on wave overtopping based on physical model tests conducted recently. Although we could not achieve very high wind speed in these tests, still the conditions are found to be conducive for observing three different types of overtopping with wind effect of different order of magnitude. Much of wind effect is linked to the form of the overshooting jet which in turn is dictated by the stability of standing wave at the structure. If the overshooting jet is not so thick (the Type C overtopping), even small wind speed can cause great fragmentation of the jet, leading to overtopping discharge almost two time that without wind. Surprisingly, exact opposite trend is found immediately after the defence when the overshooting jet is thick (e.g., the Type B overtopping), where the small wind speed is more active as the jet collapses with lower kinetic energy than the overshooting jet due to standing waves. This causes to have more wind effects at some distance from the sea defence. Overall, we find that the wind speed we are able to achieve, is most influential in smaller incident wave heights. The dynamics of the wind interaction with thick overshooting jet and with very high speed can be more complex where we might need to resolve the mixing properly by a proper turbulence model. Once the results from the CFD simulations are fully validated, we can use them as basis for developing a large data base to answer wind effects on wave overtopping in practical Coastal Engineering.

ACKNOWLEDGEMENTS

This project was funded and supported by the Natural Environment Research Council (NERC), UK under grant No. NE/R009155/1 and the Construction Industry Research and Information Association (CIRIA), UK, to whom we are very grateful. We are also grateful for the NOC through the WireWall NERC project (NE/R014019/1).

APPENDIX

We use the open source CFD library OpenFOAM® in order to simulate wind effects on the wave overtopping. OpenFOAM solves Reynolds-Averaged Navier-Stokes (RANS) equations, which in vector form read:

$$\nabla \cdot \mathbf{u} = 0, \quad (2)$$

$$\frac{\partial \rho \mathbf{u}}{\partial t} + \nabla \cdot (\rho \mathbf{u} \mathbf{u}) - \nabla \cdot \boldsymbol{\tau} = -\mathbf{g} \cdot \mathbf{x} \nabla \rho - \nabla p_d, \quad (3)$$

where \mathbf{u} is the velocity vector having three components, \mathbf{x} is the radius vector in a Cartesian coordinate system, ρ is the density of the air and water mixture. The pseudo-dynamic pressure $p_d = p - \rho \mathbf{g} \cdot \mathbf{x}$ is the static pressure minus the hydrostatic component. The stress tensor is

$$\boldsymbol{\tau} = (\mu + \mu_t) [\nabla \mathbf{u} + (\nabla \mathbf{u})^T], \quad (4)$$

where μ is the dynamic viscosity and μ_t is the turbulent viscosity to be determined from the appropriate semi-empirical turbulence model. We modify the pressure gradient in order to have desired wind speed in

a given region of the computational domain using cell zones based on underlying finite volume cells. It is important to note that the turbulence model is applied in cases when the air or water flows are strongly turbulent in the entire computational domain. In our case, the effects of turbulence are significant only in the small region where the wind flow is induced numerically. In other regions of the domain, the turbulence is weak and cannot be accounted for using semi-empirical turbulence models, thus we select $\mu_t = 0$.

The motion of the two-phase mixture of water and air with the sharp interface between the phases is taken into account using the Volume of Fluid (VOF) technique by solving the phase fraction equation:

$$\frac{\partial \alpha}{\partial t} + \nabla \cdot \mathbf{u}\alpha + \nabla \cdot (\mathbf{u}_r \alpha (1 - \alpha)) = 0. \quad (5)$$

Here the volume fraction α is bounded within $[0, 1]$ with value 0 referring to a dry cell and 1 to a wet cell. Any value within the range refers to a cell at the air-water interface. The third term in (5) introduces an artificial compression that helps to maintain the air-water interface sharp by selecting $|\mathbf{u}_r| = \min [c_\alpha |\mathbf{u}|, \max(|\mathbf{u}|)]$ with the appropriate compression factor c_α . The density of mixture in (2) - (3) is $\rho = \alpha \rho_w + (1 - \alpha) \rho_a$, where ρ_w and ρ_a are densities of water and air respectively. The Finite Volume Method (FVM) was used to solve the equations (2) - (5). For a water wave simulation one key issue is wave generation at the inlet and its absorption at the outlet for carrying out simulations for a sufficiently long time. For that purpose in the present study, we use the set of libraries named waves2Foam (Jacobsen et al. (2012)). All the simulations are performed using the OpenFOAM ESI version 1706.

References

- J. De Rouck, J. Geeraerts, P. Troch, A. Kortenhaus, T. Pullen, and L. Franco. New results on scale effects for wave overtopping at coastal structures. In N. W. H. Allsop, editor, *Proceedings of International Conference on Coastlines, Structures and Breakwaters*, London, UK, 2005.
- J. P. De Waal, P. Tönjes, and J. van der Meer. Wave overtopping of vertical structures including wind effect. In B. L. Edge, editor, *Proceedings of 25th Coastal Engineering Conference*, pages 2216–2229, Orlando, Florida, USA, 1996.
- J. A. González-Escrivá, J. M. Garrido, J. R. Medina, and J. Geeraerts. Laboratory real storm reproduction using wind. In J. M. Smith, editor, *Proceedings of 29th Coastal Engineering Conference*, volume 1, pages 677–689, Lisbon, Portugal, 2004.
- N. G. Jacobsen, D. Fuhrman, and J. Fredsoe. A wave generation toolbox for the open-source CFD library OpenFoam. *International Journal for Numerical Methods in Fluids*, 70(9):1073–1088, 2012.
- M.-S. Longuet-Higgins and A. Drazen. On steep gravity wave meeting a vertical wall: a triple instability. *Journal of Fluid Mechanics*, 466:305–318, 2002.
- J. Van der Meer, N. W. H. Allsop, T. Bruce, J. De Rouck, A. Kortenhaus, T. Pullen, H. Schüttrumpf, P. Troch, and B. Zanuttigh. *EurOtop. Manual on wave overtopping of sea defences and related structures. An overtopping manual largely based on European research, but for worldwide application*, 2018. URL <http://www.overtopping-manual.com>.
- M. R. A. van Gent, H. Van den Boogaard, B. Pozueta, and J. R. Medina. Neural network modelling of wave overtopping at coastal structures. *Coastal Engineering*, 54:583–593, 2007.
- G. Wolters and M. R. A. van Gent. Maximum wind effect on wave overtopping of sloped coastal structures with crest elements. In L. Franco, G. R. Tomasicchio, and A. Lamberti, editors, *Proceedings of 5th Coastal Structures Conference*, pages 1263–1274, Venice, Italy, 2007.